

TriMap: Large-scale Dimensionality Reduction Using Triplets

Ehsan Amid & Manfred K. Warmuth
 Google Research, Brain Team
 {eamid, manfred}@google.com

Abstract

We introduce “TriMap”; a dimensionality reduction technique based on triplet constraints, which preserves the global structure of the data better than the other commonly used methods such as t-SNE, LargeVis, and UMAP. To quantify the global accuracy of the embedding, we introduce a score that roughly reflects the relative placement of the clusters rather than the individual points. We empirically show the excellent performance of TriMap on a large variety of datasets in terms of the quality of the embedding as well as the runtime. On our performance benchmarks, TriMap easily scales to millions of points without depleting the memory and clearly outperforms t-SNE, LargeVis, and UMAP in terms of runtime.

[Update] The results in the current version of the paper is using an older version of the code available at: <https://github.com/eamid>. The results will be updated using version $\geq 1.1.0$ (although there will not be substantial changes in terms of quality). A JAX implementation of TriMap is also available at: <https://github.com/google/trimap>.

1 Introduction

Data visualization based on dimensionality reduction (DR) is a core problem in data analysis and machine learning. The aim of DR is to provide a low-dimensional representation (typically in 2D or 3D) of a given high-dimensional dataset that preserves the overall structure of the data as much as possible. The earlier approaches for DR involve linear methods such as PCA (Pearson, 1901). PCA aims to maintain the second-order statistics of the data by projecting the points into the low dimensional space that preserves the maximum amount of variance among all such projections. As a result, PCA has been shown to be effective in preserving the *global structure* of the data (Silva & Tenenbaum, 2003). The global structure includes the overall shape of the dataset, placement of the clusters, and the existence of potential outliers. Unlike PCA, much of the focus of the more recent non-linear methods, including t-SNE (Maaten & Hinton, 2008), LargeVis (Tang et al., 2016), and UMAP (McInnes et al., 2018) has been on preserving the local neighborhood structure of each individual point. Similarly, the common performance measures of DR such as trustworthiness-continuity (Venna & Kaski, 2005), precision-recall (i.e., AUC) (Venna et al., 2010), and nearest-neighbor accuracy have also been developed by retaining the same focus on reflecting the local accuracy of the embedding. Thus, there has been a lack of attention on developing methods that focus on preserving the global structure of the data and, likewise, practical performance measures to assess the global accuracy.

We first introduce the *global score*, a quantitative measure that reflects the closeness of a given embedding to the PCA embedding (which is optimal by means of preserving the data variance). The purpose of this score is to measure the accuracy of an embedding in reflecting the overall placement of the clusters of points relative to their original representation in high-dimension. By design, PCA yields the highest global score among all the DR methods, and high values of global score indicate the efficacy of a DR method in reflecting the global structure.

Next, we introduce *TriMap*, a DR method that focuses on preserving the global structure of the data in the embedding. Pairwise (dis)similarities between points (used by the previous DR methods) seem to be insufficient in capturing the global structure. Instead, TriMap incorporates a higher order of structure to construct the embedding by means of *triplets*:

$$(i, j, k) \Leftrightarrow \text{point } i \text{ is closer to point } j \text{ than point } k.$$

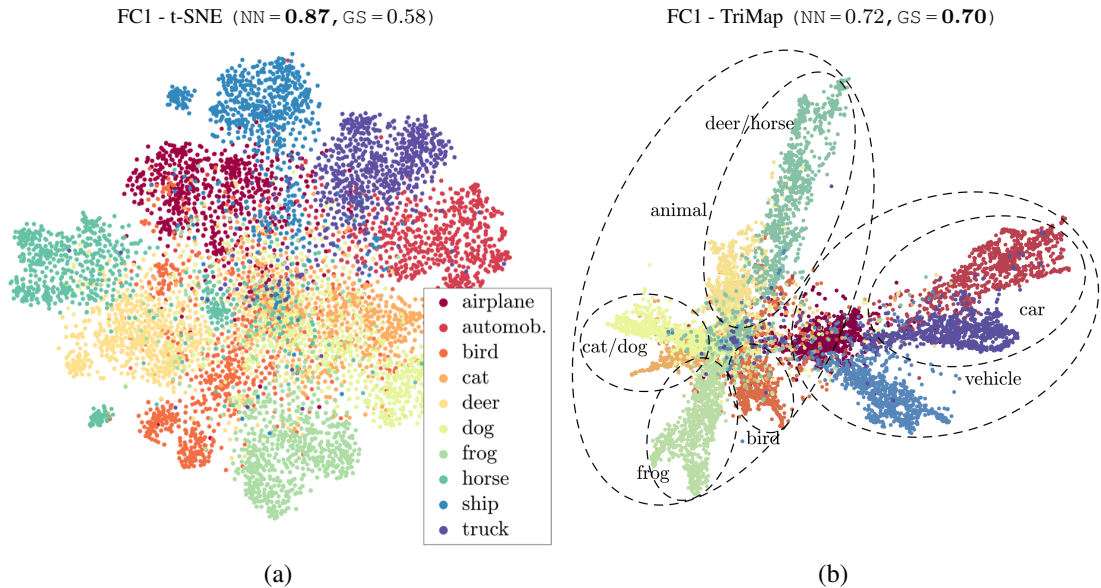


Figure 1: Visualization of the output of the first fully-connected layer of a convolutional network trained on the CIFAR-10 dataset (see the experiments section for details): (a) t-SNE, (b) TriMap. Each plot shows the embedding of the test set containing 10,000 images. The values of nearest-neighbor accuracy and global score (introduced later) are shown as a pair (AUC, GS) on top of each plot. Note that t-SNE plot fails to present the underlying structure. In contrast, TriMap plot shows multiple hierarchies in the data: the two super-clusters corresponding to “animal” and “vehicle” as well as multiple smaller clusters are successfully uncovered. Note that a higher GS value for TriMap reflects this fact.

The key idea behind TriMap stems from semi-supervised metric learning (Amid et al., 2016): Given an initial low-dimensional representation for the data points, the triplet information from the high-dimensional representation of the points is used to enhance the quality of the embedding. Similarly, TriMap is initialized with the low dimensional PCA embedding and this embedding is then modified using a set of carefully selected triplets from the high-dimensional representation.

With an extensive set of experiments, we show that TriMap produces excellent results on a variety of real-world as well as synthetic datasets. We show that in many cases, TriMap outperforms all the competitor non-linear methods by means of the global score and provides comparable local accuracy. While being significantly faster than t-SNE, TriMap provides comparable runtime to UMAP and LargeVis while scaling drastically better to larger datasets. On the Character Font Images dataset of $\sim 1.7M$ points, TriMap calculates the embedding in ~ 1.3 hours while LargeVis takes more than 3 hours and UMAP exceeds the 12 hours time limit. Our contributions can be summarized as follows:

- We introduce a global score to quantify the quality of a low-dimensional embedding in reflecting the global structure of the high-dimensional data, such as placement of the clusters rather than the local neighborhood of individual points.
- We introduce TriMap, a fast dimensionality reduction method that provides embeddings of the data that are globally more accurate than other non-linear DR methods such as t-SNE, LargeVis, and UMAP.
- We provide an efficient implementation¹ of TriMap that can easily scale to millions of points on commodity hardware and outperforms the competing methods in terms of runtime. We also perform many large-scale experiments on various datasets to show the efficacy of TriMap in terms of DR performance measures and runtime. [Update] A JAX implementation of TriMap is available at: <https://github.com/google/trimap>.

¹<https://github.com/eamid>

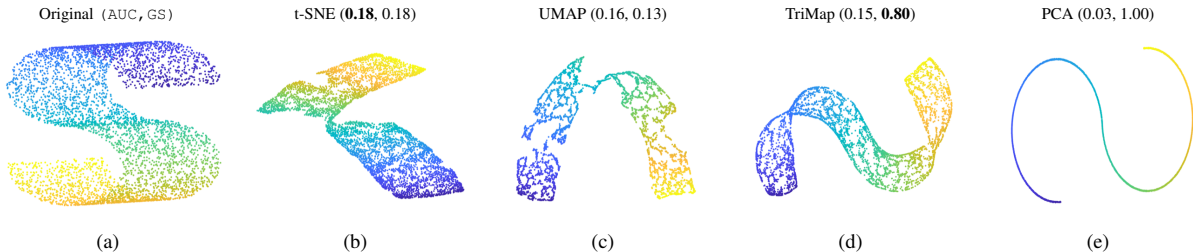


Figure 2: 2-D Visualizations of the S-curve dataset: (a) original dataset in 3-D, (b) t-SNE, (c) UMAP, (d) TriMap, and (e) PCA. The AUC and global score values for, respectively, measuring local and global accuracy, are shown in order as a pair (AUC, GS) for each embedding. Despite having higher AUC values, t-SNE and UMAP both fail to reflect the overall shape of the S-curve. On the other hand, TriMap successfully unveils the underlying structure in the original dataset. GS is the only DR performance measure that can reflect this property.

2 A Measure of Global Accuracy

Consider the S-curve dataset² which consists of 5000 points in 3-D uniformly sampled from an S-shaped manifold (Figure 2.(a)). This dataset serves as a paradigmatic problem for evaluating the performance of DR methods. In Figure 2, we show the results of 2-D embeddings of the S-curve dataset using t-SNE, UMAP, TriMap, and PCA. The top of each graph is labeled by the scoring pair (AUC, GS) where GS stands for global score (introduced below). Note that both t-SNE and UMAP provide higher values of the AUC score and locally preserve the continuity of the manifold. However, they both fail to recover the global structure of the S-curve, which is naturally reflected in the PCA embedding. On the other hand, our TriMap method (formally defined later) successfully recovers the structure of the S-curve by “unveiling” the curved shape of the manifold at both ends. Overall, the 2-D TriMap embedding resembles the original 3-D representation as much as possible. Note also that GS is the only measure that can reflect the global accuracy of the embedding.

The previous example indicates that the local measures of DR performance (such as AUC) cannot reflect the global accuracy of a low-dimensional embedding. In fact, the low-granular structure of the data can only be estimated by considering the global statistics of the dataset, as regarded by the PCA method. PCA is a linear DR method that projects the high-dimensional data onto the top- d orthogonal directions having the highest variance. In order to calculate the mapping, PCA only considers the aggregate statistics of the dataset rather than the local information of each individual data point. As a result, PCA is extremely well suited at retaining the *global structure* of the data, i.e., the overall shape of the dataset, placement of the clusters, and the existence of potential outliers. However, by focusing on the global structure, PCA loses much of the local information, such as the neighborhood structure of each data point.

Given a low-dimensional mapping produced by PCA, it is possible to calculate an optimal inverse mapping into the original high-dimensional space by means of minimizing the squared error. The optimal inverse map also corresponds to a linear mapping.³ In order to quantify the global accuracy of a DR result, we focus on the accuracy of the embedding in reflecting the global structure of the data similar to PCA. That is, we consider the minimum reconstruction error of the original dataset by means of a linear inverse map. Given n data points $\{\mathbf{x}_i \in \mathbb{R}^m\}_{i=1}^n$, let $\mathbf{X} \in \mathbb{R}^{m \times n}$ denote the high-dimensional data matrix where the i -th column corresponds to \mathbf{x}_i . Similarly, let $\mathbf{Y} \in \mathbb{R}^{d \times n}$ denote the matrix of the low-dimensional embedding of the points $\{\mathbf{y}_i \in \mathbb{R}^d\}_{i=1}^n$. Without loss of generality, we assume both \mathbf{X} and \mathbf{Y} are centered. We define the *Minimum Reconstruction Error (MRE)* from the embedding as

$$\mathcal{E}(\mathbf{Y} | \mathbf{X}) := \min_{\mathbf{A} \in \mathbb{R}^{m \times d}} \|\mathbf{X} - \mathbf{A}\mathbf{Y}\|_F^2,$$

where $\|\cdot\|_F$ denotes the Frobenius norm.⁴ Note that PCA has the lowest possible MRE among all the DR methods. Thus, in order to obtain a normalized measure of global accuracy of a given embedding \mathbf{Y} for a data \mathbf{X} , we define the

²https://scikit-learn.org/stable/modules/generated/sklearn.datasets.make_s_curve.html

³More specifically, mapping to low-dimension corresponds to projecting the data onto the top- d eigendirections of the data covariance matrix. The inverse mapping is induced by the transpose of the projection matrix.

⁴The optimum value \mathbf{A}^* for the MRE can be calculated efficiently as

$$\mathbf{A}^* = \mathbf{X}\mathbf{Y}^\top(\mathbf{Y}\mathbf{Y}^\top)^{-1}.$$

This also handles possible rotation and scaling of the embedding.

global score (GS) as

$$\text{GS}(\mathbf{Y}|\mathbf{X}) := \exp\left(-\frac{\mathcal{E}(\mathbf{Y}|\mathbf{X}) - \mathcal{E}_{\text{PCA}}}{\mathcal{E}_{\text{PCA}}}\right) \in [0, 1],$$

where $\mathcal{E}_{\text{PCA}} := \mathcal{E}(\mathbf{Y}_{\text{PCA}}|\mathbf{X})$ denotes the MRE achieved by the PCA embedding \mathbf{Y}_{PCA} on the same dataset \mathbf{X} . Note that $\text{GS}(\mathbf{Y}_{\text{PCA}}|\mathbf{X}) = 1$ and we suggest that larger values of GS indicate a higher capacity of a DR method to reflect the global structure of the data, as shown in the experiments.

In the remainder of the paper, we use GS as the global performance measure. Due to the high computational complexity for calculating the trustworthiness-continuity and AUC scores for large data sets, we use nearest-neighbors accuracy as the local measure of performance henceforth.

3 The TriMap Method

We now formally introduce the TriMap method. Recall that a triplet consists of three points (i, j, k) where point i is closer to point j than point k . TriMap chooses a subset $\mathcal{T} = \{(i, j, k)\}$ of triplets and assigns a weight $\omega_{ijk} \geq 0$ for each triplet: a higher value of ω_{ijk} implies that the pair (i, k) is located much farther than the pair (i, j) . We define the loss of the triplet (i, j, k) as

$$\ell_{ijk} := \omega_{ijk} \frac{s(\mathbf{y}_i, \mathbf{y}_k)}{s(\mathbf{y}_i, \mathbf{y}_j) + s(\mathbf{y}_i, \mathbf{y}_k)}, \quad \text{where } s(\mathbf{y}_i, \mathbf{y}_j) = (1 + \|\mathbf{y}_i - \mathbf{y}_j\|^2)^{-1},$$

is a similarity function between \mathbf{y}_i and \mathbf{y}_j . The choice of s is motivated by the good performance of Student t-distribution for similarities in low-dimension in the t-SNE method. Note that the loss of the triplet (i, j, k) approaches zero as $\|\mathbf{y}_i - \mathbf{y}_j\|$ decreases and $\|\mathbf{y}_i - \mathbf{y}_k\|$ increases.

We first develop the weighing scheme for the triplets. To reflect the relative similarities in high-dimension, we define the weight of the triplet (i, j, k) as

$$\tilde{\omega}_{ijk} = d_{ik}^2 - d_{ij}^2 \geq 0,$$

in which, d_{ij} is any distance measure between \mathbf{x}_i and \mathbf{x}_j in high-dimension. As the default distance, we consider the squared Euclidean distance. We also apply the scaling introduced in (Zelnik-Manor & Perona, 2005),

$$d_{ij}^2 = \frac{\|\mathbf{x}_i - \mathbf{x}_j\|^2}{\sigma_{ij}},$$

where $\sigma_{ij} = \sigma_i \sigma_j$ and σ_i is set to the average Euclidean distance between \mathbf{x}_i and the set of nearest-neighbors of \mathbf{x}_i from 4-th to 6-th neighbors. This choice of σ_{ij} adaptively adjusts the scaling based on the density of the data.

[Update] We shift the final weights by subtracting the minimum weight value calculated over all triplets and applying a tempered log transformation,

$$\omega_{ijk} = \log_t(1 + \tilde{\omega}_{ijk} - \omega_{\min}),$$

where $\omega_{\min} = \min_{(i', j', k') \in \mathcal{T}} \tilde{\omega}_{i'j'k'}$, and

$$\log_t(u) = \frac{1}{1-t} (u^{1-t} - 1), \quad t \neq 1,$$

is called the tempered logarithm (Naudts, 2002). The \log_t transformation smoothens the weights and prevents the triplets with large weights from dominating the total loss. Note that the limit case $t \rightarrow 1$ recovers the standard log. We use $t = 0.5$ as the default value.

To construct the embedding, we consider a small subset of all possible triplets (i, j, k) for which the closer point j belongs to the set of nearest-neighbors of the point i and the farther point k is among the points that are more distant from i than j , chosen uniformly at random. For each point we consider its $m = 10$ nearest neighbors and sample $m' = 5$ triplets per nearest-neighbor. This yields $m \times m' = 50$ nearest-neighbor triplets per point. In addition, we also add $r = 5$ random triplets (i, j, k) per each point i where j and k are sampled uniformly at random and their order is

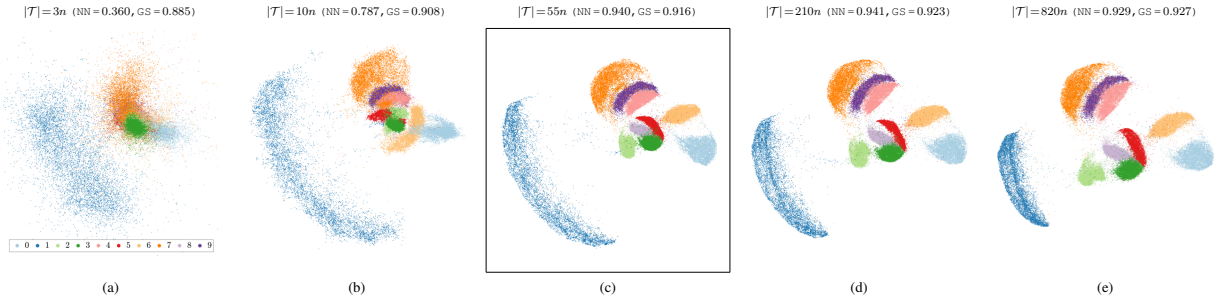


Figure 3: Effect of changing the number of triplets on the quality of the embeddings of the MNIST dataset. We consider $(m, m', r) = c \times (2, 1, 1)$ for: (a) $c = 1$, (b) $c = 2$, (c) $c = 5$ (default) [Update] The new default values are $(m, m', r) = (12, 4, 3)$, (d) $c = 10$, and (e) $c = 20$. The values of nearest neighbor accuracy and global score are shown as a tuple (NN, GS) on top of each figure. The quality of embedding does not improve significantly after adding a certain number of triplets.

Dataset	t-SNE		UMAP		TriMap		PCA	
	PCC	GS	PCC	GS	PCC	GS	PCC	GS
COIL-20	0.56	0.63	0.30	0.52	0.50	0.69	0.88	1.00
USPS	0.70	0.89	0.88	0.90	0.85	0.93	0.91	1.00
Epileptic S.	0.69	0.91	0.82	0.90	0.91	0.91	0.84	1.00
Tabula M.	0.56	0.05	0.30	0.09	0.82	0.17	0.93	1.00
MNIST	0.62	0.90	0.79	0.91	0.77	0.92	0.83	1.00
Fashion MNIST	0.66	0.53	0.90	0.75	0.92	0.87	0.97	1.00

Table 1: Comparison of the Pearson correlation coefficient (PCC) and global score (GS) values for different method. Overall, TriMap yields higher scores than t-SNE. Notice the strong correlation between PCC and GS.

possibly switched based on their nearness to i . This yields $m \times m' + r = 55$ triplets per point in total. ([Update] The new default parameters are set to $m = 12$, $m' = 4$, and $r = 3$.) Thus, the overall complexity of the optimization step is linear in number of points n . The computational complexity is dominated by the nearest-neighbor search, which is shared among all the recent methods such as t-SNE, LargeVis, and UMAP. We use ANNOY for the approximate nearest-neighbor search⁵ which is based on random projection trees.

While a random initialization for the embedding also works well in practice, we initialize the embedding to the PCA solution \mathbf{Y}_{PCA} (scaled by a small constant value for better convergence). The PCA initialization for TriMap allows faster convergence while preserving much of the global structure discovered by PCA. Note that the other DR methods such as t-SNE are extremely sensitive to the initialization and do not converge well with any initial solution other than small random initialization around the origin.

We define the final loss as the sum of the losses of the sampled triplets in \mathcal{T}

$$\ell_{\text{TriMap}} = \sum_{(i,j,k) \in \mathcal{T}} \ell_{ijk}.$$

The loss is minimized using the full-batch gradient descent with momentum using the delta-bar-delta method. In all our experiments, we perform 400 iterations with the value of momentum parameter equal to 0.5 during the first 250 iterations and 0.8 afterwards.

Finally, note that there exist connections between TriMap and a number of *triplet (aka ordinal) embedding* methods such as t-STE (Van Der Maaten & Weinberger, 2012). The triplet embedding methods have been developed for a different setting where the goal is to find an embedding based on a given pre-specified set of triplets obtained from human evaluators (or some form of implicit feedback). For instance, t-STE maximizes the sum of log of the satisfaction probabilities of the triplets to calculate the embedding. It is worth mentioning that TriMap is a DR method

⁵<https://github.com/spotify/annoy>. [Update] The JAX implementation uses PyNNDescent: <https://github.com/lmcinnes/pynndescent>.

Dataset (size)	t-SNE	LargeVis	UMAP	TriMap	Speedup
COIL-20 (1440)	00:00:08	00:05:51	00:00:04	00:00:02	2.00×
USPS (11K)	00:02:02	00:06:12	00:00:12	00:00:11	1.10×
Epileptic Seizure (11.5K)	00:03:11	00:06:17	00:00:15	00:00:12	1.25×
20 Newsgroup (18K)	00:05:34	00:06:57	00:00:26	00:00:21	1.24×
Tabula Muris (54K)	00:17:32	00:09:29	00:01:12	00:01:06	2.00×
MNIST (70K)	00:20:38	00:11:29	00:01:15	00:01:23	0.90×
Fashion MNIST (70K)	00:19:10	00:11:04	00:01:18	00:01:24	0.93×
TV News (~129K)	00:38:59	00:16:26	00:02:57	00:02:45	1.07×
360+K Lyrics (~360K)	08:50:49	00:44:16	00:25:23	00:13:49	1.84×
Coverttype (~581K)	–	00:44:54	02:59:41	00:24:42	1.82×
RCV1 (800K)	–	01:34:38	04:55:53	00:36:59	2.56×
Character Font Images (~1.7M)	–	03:16:19	–	01:17:50	2.52×
KDDCup99 (~4.9M)	–	–	–	04:17:01	–
HIGGS (11M)	–	–	–	10:08:36	–

Table 2: Runtime of the methods in `hh:mm:ss` format on single machine with 2.6 GHz Intel Core i5 CPU and 16 GB of memory. We limit the runtime of each method to 12 hours. Also, UMAP runs out of memory on datasets larger than ~4M points.

that is designed to sample the informative triplets from the high-dimensional representation of a set of points and assign weights to these triplets to reflect the relative similarities of these points. Although TriMap can also be used for the triplet embedding task, we only focus on the DR results.⁶

3.1 Effect of Different Parameters

We briefly discuss the effect of different parameters, namely the total number of triplets $|\mathcal{T}|$ and the γ -scaled log-transformation, on the quality of the embedding. TriMap is particularly robust to the number of sampled triplets for constructing the embedding. This can be explained by the high amount of redundancy in the triplets (the triplets (i, j, k) and (i, j, k') convey the same information if k and k' are nearest neighbors and also mapped nearby). In Figure 3 we consider various values for m , m' , and r for the MNIST dataset while fixing the remaining parameters. In fact, using a large number of triplets can sometimes introduce overhead and require a larger number of iterations to converge.

4 Experiments

In this section, we apply TriMap on a set of real-world as well as synthetic datasets and compare the results to t-SNE, LargeVis, UMAP, and PCA methods. The datasets used in our experiments are listed in Table 2 and a short description is given in the appendix. All experiments are conducted on a single machine with 2.6 GHz Intel Core i5 CPU and 16 GB of memory. We limit the runtime of each algorithm to 12 hours. For implementations, we use the default `sklearn` implementation for t-SNE and the official implementations of LargeVis and UMAP provided by the authors^{7,8}. Due to lack of space, we provide the comparison to the LargeVis results as well as additional TriMap results on the larger datasets in the appendix.

In order to have a fair comparison, we use the default parameter values for all methods, including ours ($m = 10$, $m' = 5$, $r = 5$, $\gamma = 500$, and 400 iterations). ([Update] The new default parameters are set to $m = 12$, $m' = 4$, $r = 3$, $t = 0.5$, and γ -scaled log-transformation has been removed.) Also, to reduce the overhead induced by the dimensionality of the data in the nearest-neighbor search step, we reduce the number of dimensions of the dataset to 100 if necessary, using the PCA method. To evaluate the local performance, we show the nearest-neighbor accuracy

⁶Also, the embeddings obtained by simply applying these methods to our set of sampled triplets are quite subpar (see the MNIST result in (Van Der Maaten & Weinberger, 2012)) and are not shown here.

⁷<https://github.com/lferry007/LargeVis>

⁸<https://github.com/lmcinnes/umap>

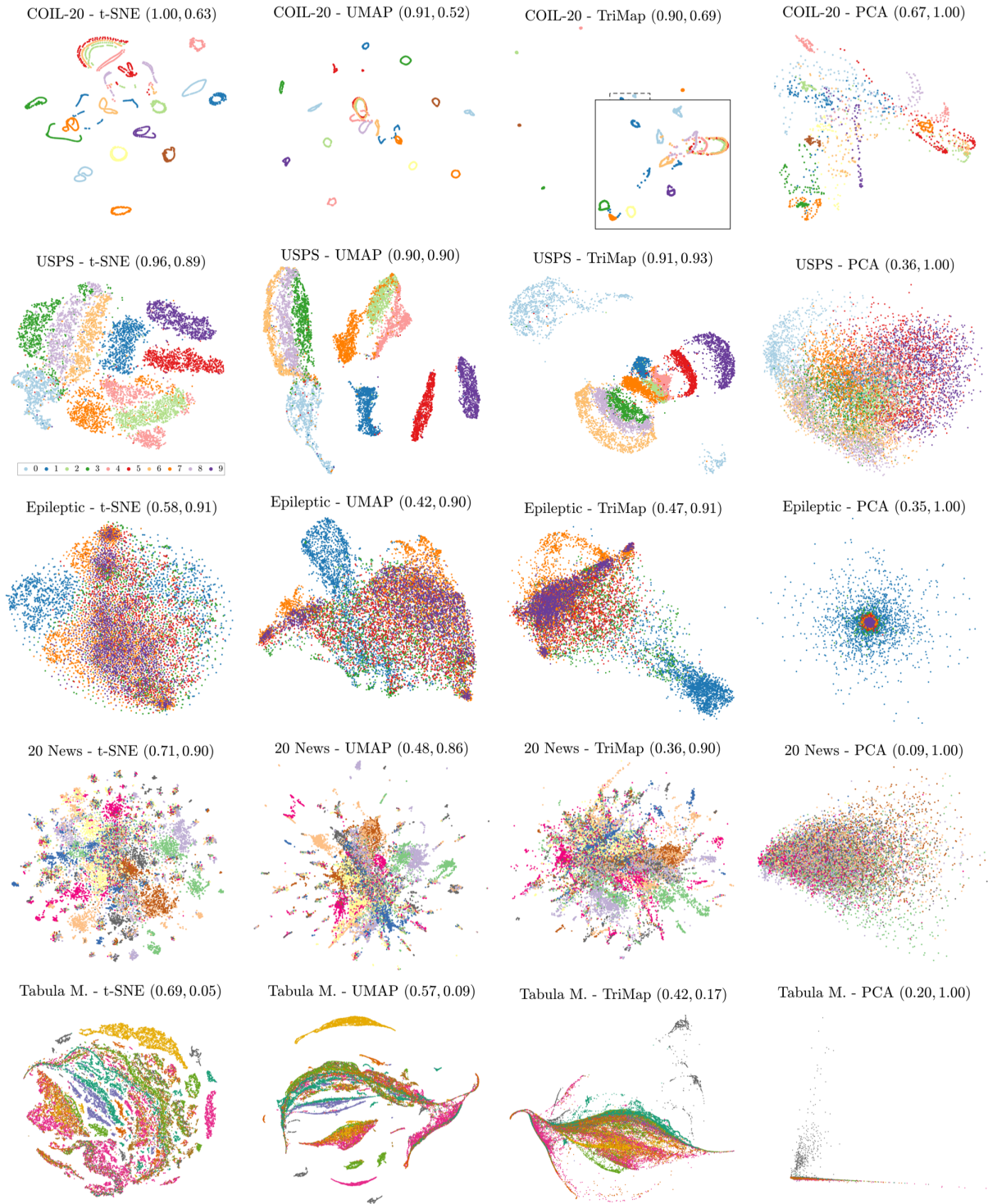


Figure 4: Visualizations of different datasets using t-SNE, UMAP, TriMap, and PCA. Each row corresponds to one dataset and each column represents one method. The values of nearest neighbor accuracy and global score are shown as a pair (NN, GS) on top of each figure.

of each result. We also show the GS as a measure of global performance. The performance measures are shown on top of each figure as a pair (NN, GS).

4.1 Global Accuracy

We first validate the efficacy of the GS measure by drawing a comparison to the recently proposed Pearson Correlation Coefficient (PCC) (Freedman et al., 2007). To calculate PCC, we consider random subsets of size 10,000 from different datasets and perform k -means clustering in the high-dimensional space with $k = 100$. Next, we perform the clustering in the low-dimensional embedding on the same subset of points and calculate the score between the distance matrices of the cluster centers in the high-dimension and low-dimension using the Mantel test. We repeat the process 100 times using different sub-samples of the data. The results are shown in Table 1. As can be seen, PCC admits a high correlation with the GS. Overall, PCC and GS are the highest for PCA (GS is equal to 1 by definition). On the other hand, TriMap yields excellent global performance and results in much higher PCC and GS scores compared to t-SNE.

4.2 Visualization of Standard Datasets

The visualizations of the datasets using TriMap as well as the other competing methods are shown in Figure 4 and 5. We provide a zoomed-in snippet over the main figure for some results to provide a more detailed illustration. Overall, TriMap preserves the underlying global structure of the data better than the other competing methods. This is reflected by the larger GS values for TriMap as well as visually comparing the embeddings to the PCA result. For example, TriMap recovers the continuous structure of the TV news dataset and separates the remaining outliers in the data, which are also identified by the PCA method. This can be verified by comparing the placement of an example outlier point, marked with a red \times , by the different methods: TriMap shows this point among other outliers, whereas t-SNE and UMAP fail to uncover this information. Also, the global score of TriMap on this dataset is much higher than the other methods. Further discussion is given in the appendix.

4.3 Runtime

The runtime of the methods are provided in Table 2 in the `hh:mm:ss` format. We limit the runtime of each method to 12 hours. As can be seen from the results, TriMap provides excellent runtime and outperforms all the other methods in most cases. Also, TriMap easily scales to millions of points while the other methods exceed the time limit or run out of memory. For instance, UMAP causes an out of memory error for datasets larger than ~ 4 M points.

4.4 Visualization of Neural Networks

We visualize the different embeddings of the test set (10,000 points) from the CIFAR-10 dataset when passed through different layers of a convolutional neural network. Specifically, the network has 3 convolutional layers, each sized 64, followed by 3 fully-connected layers of size 1024, 512, and 10, respectively. We use ReLU activations and apply batch normalization and dropout with a keep probability of 0.75 during training. We perform 25 epochs of batch size 512 using Adagrad optimizer on the 60,000 point training set. The trained network achieves 84% test accuracy. Note that the goal here is not to achieve the benchmark test accuracy but rather to observe the separation of clusters corresponding to different classes when passed through the network and to detect the highly misclassified examples. Figure 1 shows the visualization of the output of the first fully-connected layer of the network on the test set using t-SNE and TriMap. The values of nearest-neighbor accuracy and global score are shown as a pair (AUC, GS) on top of each plot. Note that t-SNE shows the different clusters correctly but fails to present the overall underlying structure. In contrast, TriMap plot shows multiple hierarchies in the data: the two super-clusters corresponding to “animal” and “vehicle” as well as multiple smaller clusters (e.g. “deer/horse”, “cat/dog”, etc.) are successfully uncovered. Note that a higher GS value for TriMap reflects this fact.

We visualize the output of the second fully-connected layer in Figure 6 (top). We can see that the clusters get separated better after passing through another layer of non-linearity. We also color the embedding based on the probability of the correct passing class, predicted by the network in Figure 6 (bottom). In the plot, the color “blue” indicates a high probability for the correct (i.e., label) class while “red” corresponds to a misclassification. In both t-SNE and TriMap embeddings, the highly misclassified points are concentrated in the center of the embedding. However, the TriMap embedding reveals some examples that are also misclassified with high confidence but are far away from the center. We show an example of such points (marked with \times) from the class “dog” which has been misclassified with

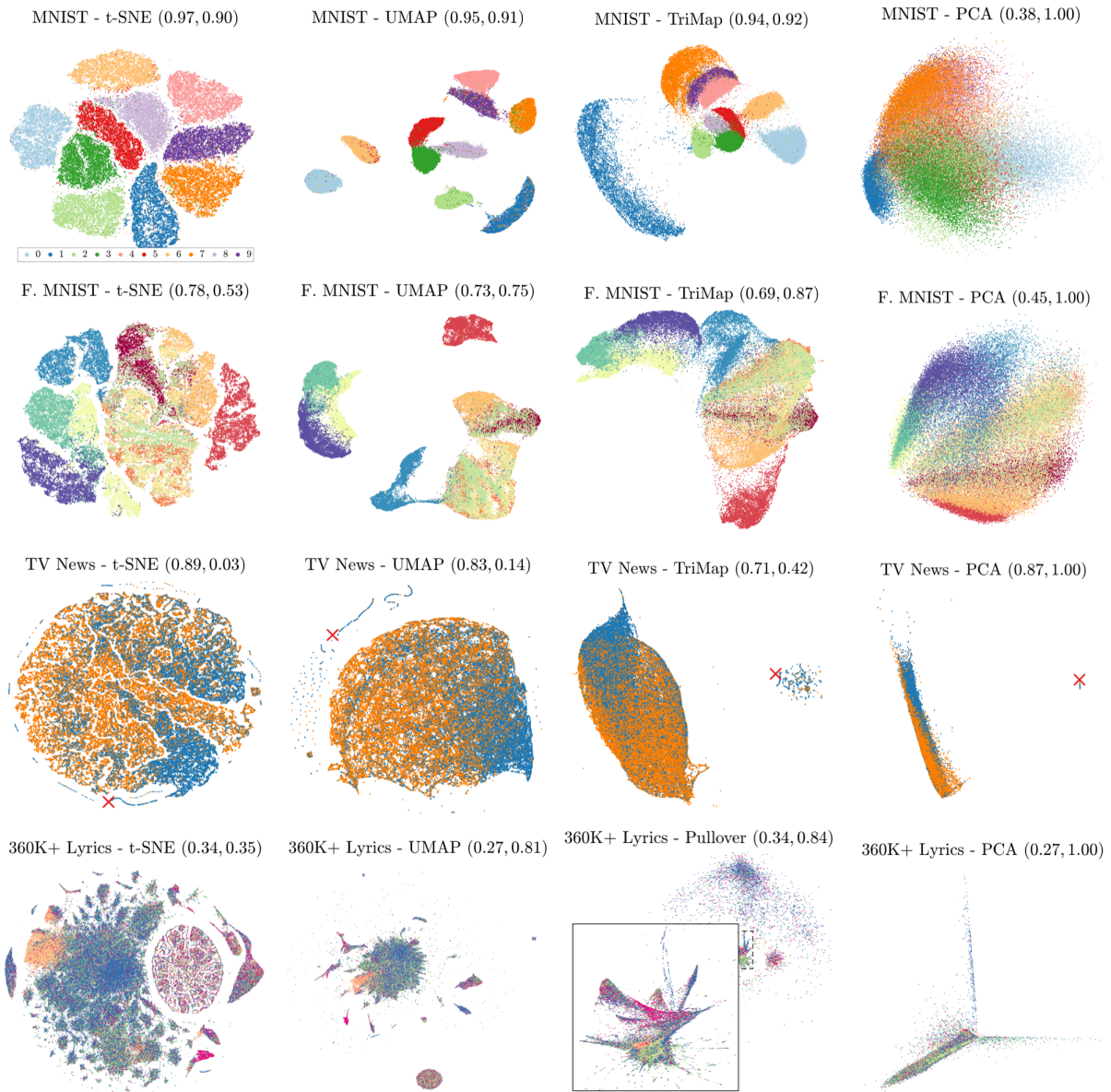


Figure 4: Visualizations of different datasets (continued) using t-SNE, UMAP, TriMap, and PCA. Each row corresponds to one dataset and each column represents one method. The values of nearest neighbor accuracy and global score are shown as a tuple (NN, GS) on top of each figure.

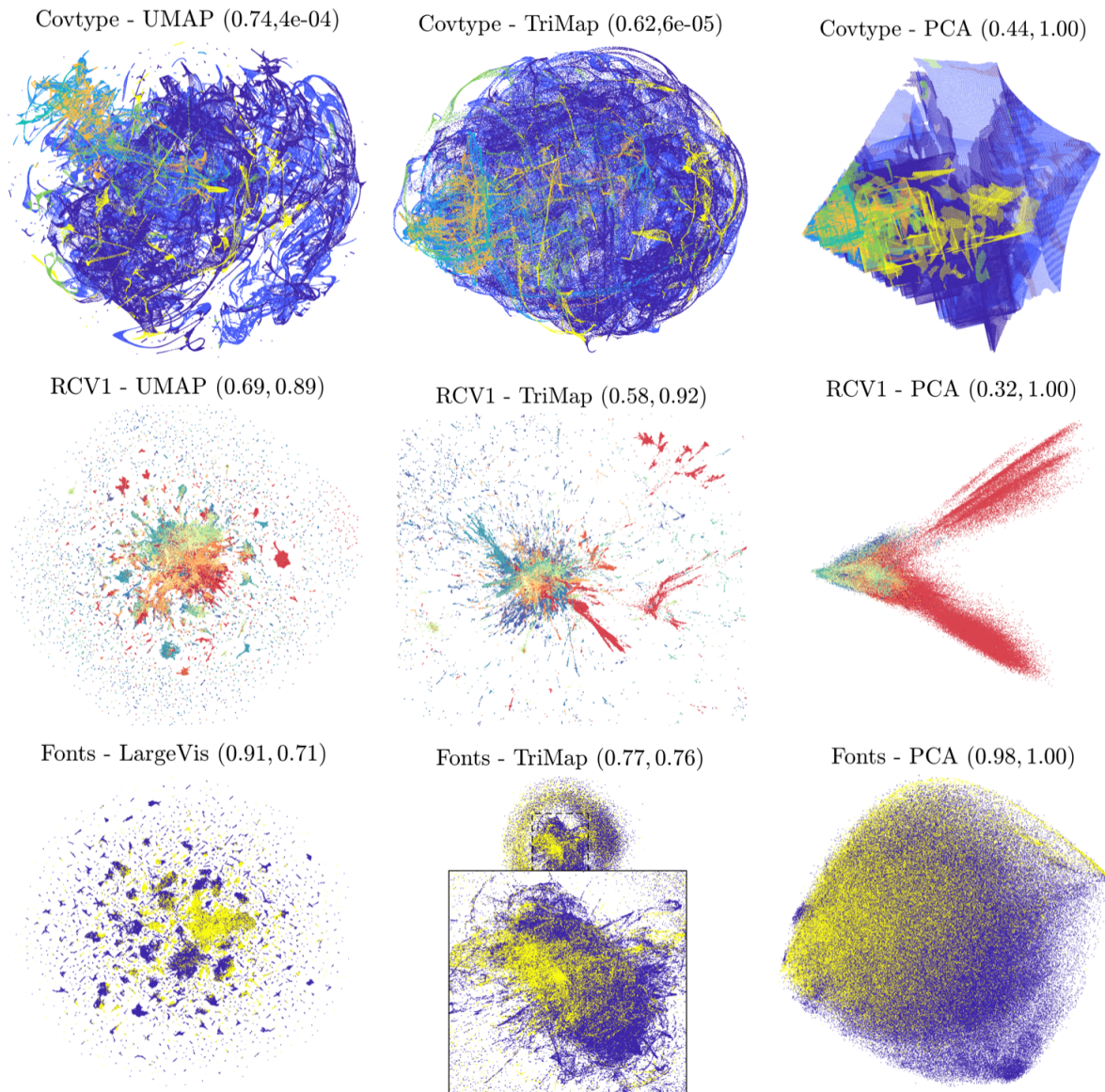


Figure 5: Visualizations of Covertype and RCV1 datasets using UMAP, TriMap, and PCA, and visualizations of the Character Font Images dataset using LargeVis, TriMap, and PCA. The values of nearest neighbor accuracy and global score are shown as a tuple (NN, GS) on top of each figure.

high confidence as class “horse” (with probability ~ 1). The same point is placed much closer to the center in the t-SNE plot, therefore not shown as a clear outlier. The actual image of the point overlaid in the TriMap plot shows the high resemblance of the example to a “horse”.

5 Conclusion and Future Work

TriMap is a fast and efficient method that can be easily applied to large datasets. While TriMap is extremely effective for uncovering the global structure of the data, other methods such as t-SNE can provide additional insight about the local neighborhood of individual points. As a future research direction, we consider using pairwise constraints along with triplet constraints to improve the local accuracy. The current implementation of TriMap utilizes a single core. Parallel implementation of the method that can exploit multiple cores is another future direction. Furthermore, the global accuracy is measured in terms of the global score, which is based on the assumption that linear projection

FC2 - t-SNE (NN = **0.87**, GS = 0.61)

FC2 - TriMap (NN = 0.77, GS = **0.84**)

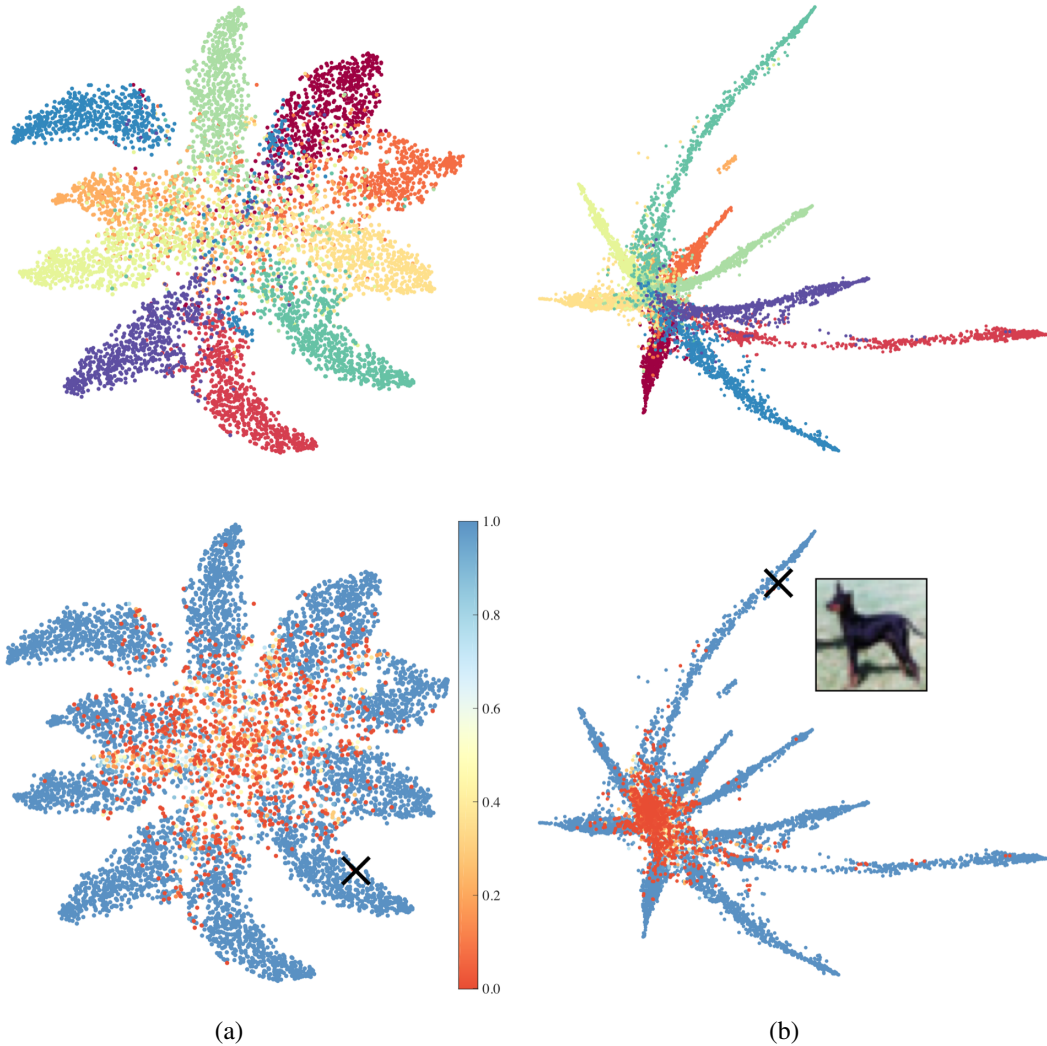


Figure 6: Visualization of the output of the second fully-connected layer: (a) t-SNE, (b) TriMap. We can observe that the clusters get separated better after passing through another layer of non-linearity. The bottom plot is colored based on the probability of the correct class. An example of a highly misclassified example from the class “dog” (classified as “horse”) is marked with \times . The point is placed much closer to the center in the t-SNE plot, therefore not shown as a clear outlier. The actual image of the point is overlaid in the TriMap plot. The higher value of GS reflects the better global accuracy of TriMap.

obtained by PCA is globally optimal. While our global score can provide insight into the global accuracy of the embedding in many cases, it appears to be ineffective when the data is highly non-linear or contains a large number of outliers. Developing non-linear and more robust global performance measures could significantly improve the assessment of the DR results and provide guidelines for developing more accurate DR techniques.

References

- Ehsan Amid, Aristides Gionis, and Antti Ukkonen. Semi-supervised kernel metric learning using relative comparisons. *arXiv preprint arXiv:1612.00086*, 2016.
- David Freedman, Robert Pisani, and Roger Purves. Statistics (international student edition). *Pisani, R. Purves, 4th edn. WW Norton & Company, New York, 2007.*

- Laurens van der Maaten and Geoffrey Hinton. Visualizing data using t-sne. *Journal of machine learning research*, 9 (Nov):2579–2605, 2008.
- Leland McInnes, John Healy, and James Melville. Umap: Uniform manifold approximation and projection for dimension reduction. *arXiv preprint arXiv:1802.03426*, 2018.
- Jan Naudts. Deformed exponentials and logarithms in generalized thermostatics. *Physica A*, 316:323–334, 2002. URL <http://arxiv.org/pdf/cond-mat/0203489>.
- Karl Pearson. Liii. on lines and planes of closest fit to systems of points in space. *The London, Edinburgh, and Dublin Philosophical Magazine and Journal of Science*, 2(11):559–572, 1901.
- Vin D Silva and Joshua B Tenenbaum. Global versus local methods in nonlinear dimensionality reduction. In *Advances in neural information processing systems*, pp. 721–728, 2003.
- Jian Tang, Jingzhou Liu, Ming Zhang, and Qiaozhu Mei. Visualizing large-scale and high-dimensional data. In *Proceedings of the 25th international conference on world wide web*, pp. 287–297. International World Wide Web Conferences Steering Committee, 2016.
- Laurens Van Der Maaten and Kilian Weinberger. Stochastic triplet embedding. In *2012 IEEE International Workshop on Machine Learning for Signal Processing*, pp. 1–6. IEEE, 2012.
- Jarkko Venna and Samuel Kaski. Local multidimensional scaling with controlled tradeoff between trustworthiness and continuity. In *Proceedings of 5th Workshop on Self-Organizing Maps*, pp. 695–702. Citeseer, 2005.
- Jarkko Venna, Jaakko Peltonen, Kristian Nybo, Helena Aidos, and Samuel Kaski. Information retrieval perspective to nonlinear dimensionality reduction for data visualization. *Journal of Machine Learning Research*, 11(Feb):451–490, 2010.
- Lihi Zelnik-Manor and Pietro Perona. Self-tuning spectral clustering. In *Advances in neural information processing systems*, pp. 1601–1608, 2005.

A Datasets

The datasets used in the experiments are listed below. All datasets are publicly available online and a download link is provided.

- **COIL-20**⁹ (1440): gray-scale images of 20 objects in uniformly sampled orientations (5 degrees of rotation, 72 images per object). Each image is pre-processed by having the background removed and cropped into size 128×128 .
- **USPS**¹⁰ (11K): images of handwritten digits (0–9) of size 16×16 .
- **Epileptic Seizure**¹¹ (11.5K): EEG signal recordings of brain activity for seizure recognition. It contains 178-dimensional vectors belonging to 5 categories.
- **20 Newsgroup**¹¹ (18K): newsgroup posts categorized into 20 topics. We use a TF-IDF representation of the words in each document as the features.
- **Tabula Muris**¹² (~54K): single cell transcriptome data from the mouse from 20 organs.
- **MNIST**¹³ (70K): images of handwritten digits (0–9) of size 28×28 .
- **Fashion MNIST**¹⁴ (70K): gray-scale images of clothing items such as t-shirt, pullover, bag, etc. of size 28×28 .
- **TV News**¹¹ (~129K): audio-visual features from TV news broadcast categorized into commercial and non-commercial.
- **360K+ Lyrics**¹⁵ (~362K): lyrics of songs from 12 different genres. We group similar genres together (metal-rock, R&B-pop, etc.) to form 7 groups. We use the TF-IDF representation of the words in the song as the features.
- **Covertypes**¹¹ (~581K): cartographic features for forest cover type prediction.
- **RCV1**¹⁶ (800K): Reuters Corpus Volume I archive of categorized newswire stories.
- **Character Font Images**¹¹ (~1.7M): images of character from scanned and computer generated fonts.
- **KDDCup99**¹¹ (~4.9M): computer network intrusion detection.
- **HIGGS**¹¹ (11M): Higgs bosons recognition from a background process.

B More Visualizations

We compare the results of TriMap to LargeVis in Figure 7 and 8. We also provide more visualizations obtained using TriMap in Figure 9.

C Discussion

We briefly discuss the results of TriMap and draw a comparison to the other methods.

TriMap generally provides better global accuracy compared to the competing methods. It also successfully maintains the continuity of the underlying manifold. This can be seen from the COIL-20 result, where certain clusters are located farther away from the remaining clusters. However, the underlying structure for the main cluster resembles the one provided by the other methods. TriMap also preserves the continuous structure in the Fashion MNIST and the TV News datasets.

⁹<http://www.cs.columbia.edu/CAVE/software/softlib/coil-20.php>

¹⁰<https://www.kaggle.com/bistaumanga/usps-dataset>

¹¹<http://archive.ics.uci.edu/ml/index.php>

¹²<https://tabula-muris.ds.czbiohub.org/>

¹³<http://yann.lecun.com/exdb/mnist/>

¹⁴<https://github.com/zalandoresearch/fashion-mnist>

¹⁵<https://www.kaggle.com/gyani95/380000-lyrics-from-metrolyrics>

¹⁶<https://scikit-learn.org/0.18/datasets/rcv1.html>

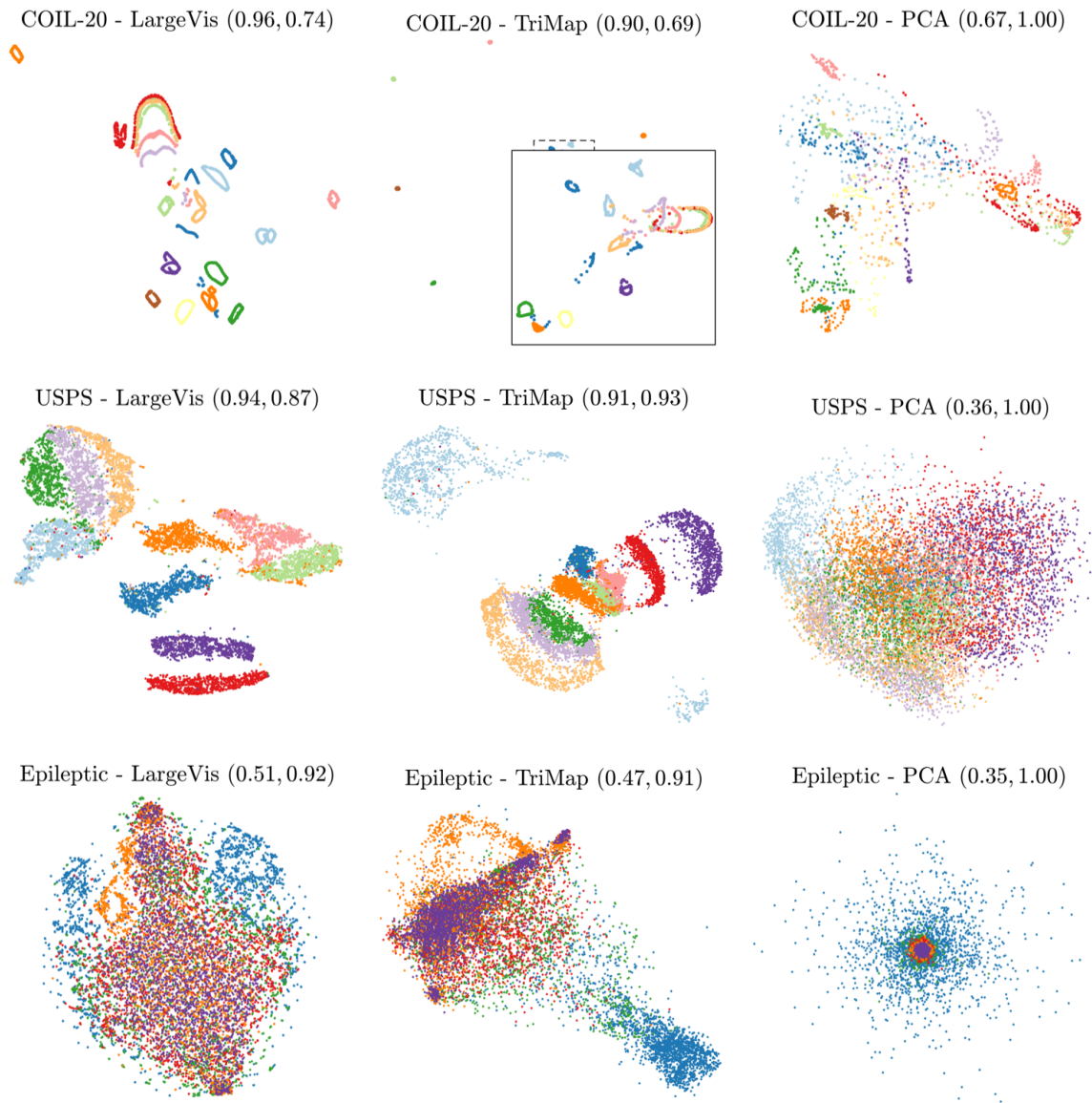


Figure 7: Visualizations of different datasets using LargeVis, TriMap, and PCA. Each row corresponds to one dataset and each column represents one method. The values of nearest neighbor accuracy and global score are shown as a pair (NN, GS) on top of each figure.

TriMap is also efficient in uncovering the possible outliers in the data. For instance, PCA reveals a large number of outliers in the Tabula Muris and the 360+K Lyrics datasets. These outliers are located far away from the main clusters in the TriMap results. However, the same points are located very close to the remaining points in the t-SNE results.

Additionally, both t-SNE and LargeVis tend to form spurious clusters by splitting the underlying connected manifold. This can be seen from the TV News results and the result of LargeVis on the Covertypes dataset.

Finally, notice that in some cases GS fails to reflect the global accuracy of the embeddings. This can be seen from the low GS values for all methods on the Covertypes dataset. GS may become uninformative when there exists a high degree of non-linearity in the data that cannot be reflected using PCA. GS also cannot reflect the accuracy of the embedding in uncovering single outliers. Developing more accurate global measures for these scenarios is a future research direction.

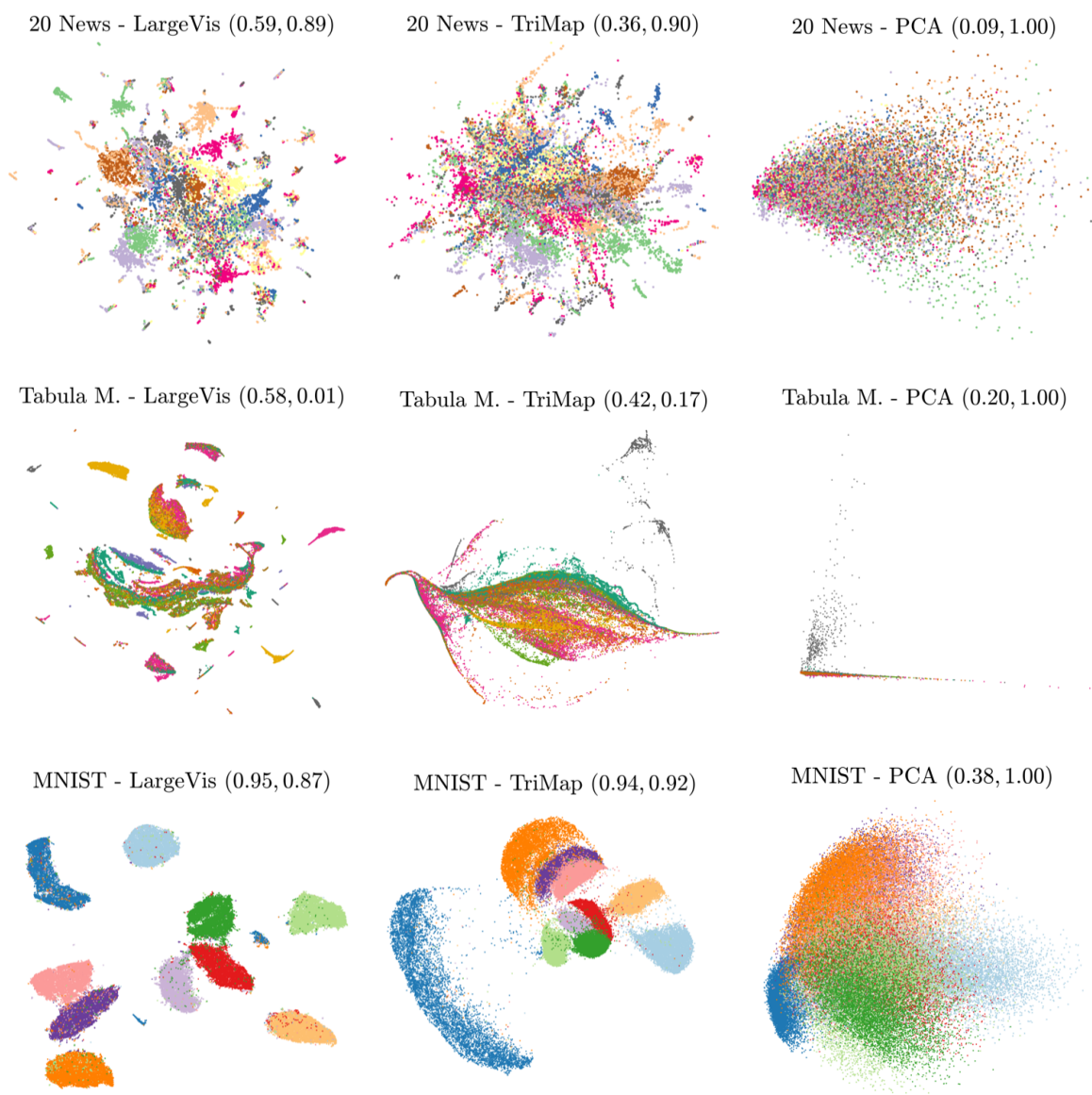


Figure 7: Visualizations of different datasets (continued) using LargeVis, TriMap, and PCA. Each row corresponds to one dataset and each column represents one method. The values of nearest neighbor accuracy and global score are shown as a pair (NN, GS) on top of each figure.

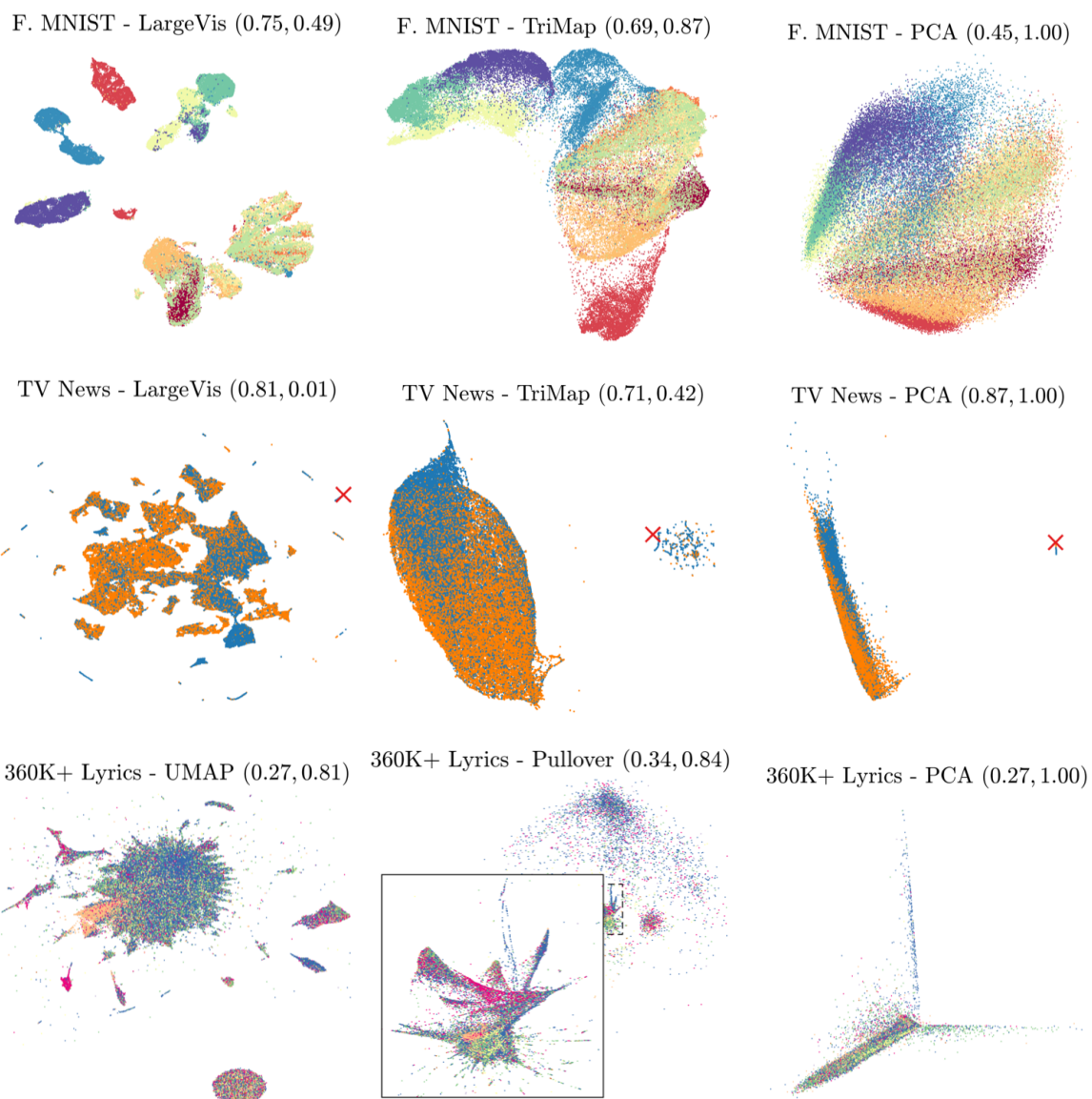
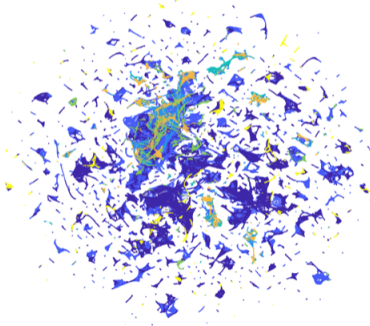
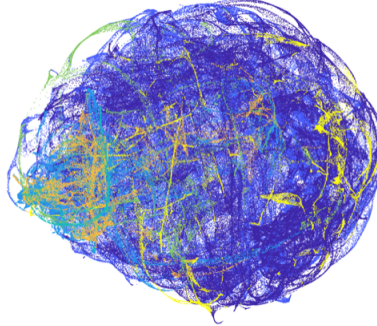


Figure 7: Visualizations of different datasets (continued) using LargeVis, TriMap, and PCA. Each row corresponds to one dataset and each column represents one method. The values of nearest neighbor accuracy and global score are shown as a tuple (NN, GS) on top of each figure.

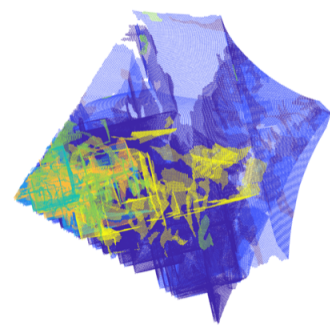
Covtype - LargeVis (0.82, 0.00)



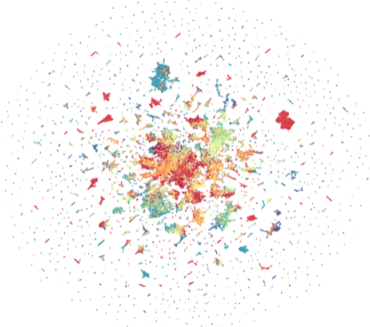
Covtype - TriMap (0.62, 6e-05)



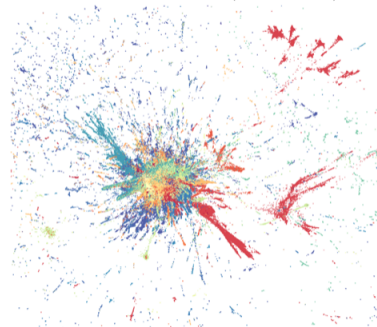
Covtype - PCA (0.44, 1.00)



RCV1 - LargeVis (0.71, 0.88)



RCV1 - TriMap (0.58, 0.92)



RCV1 - PCA (0.32, 1.00)

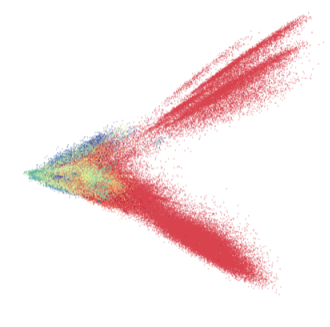
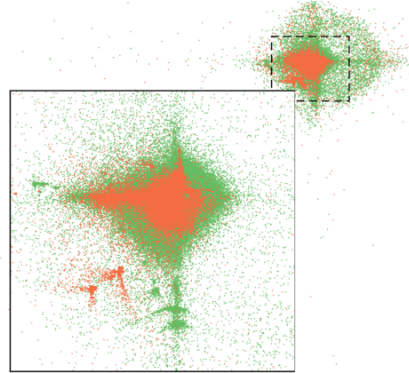
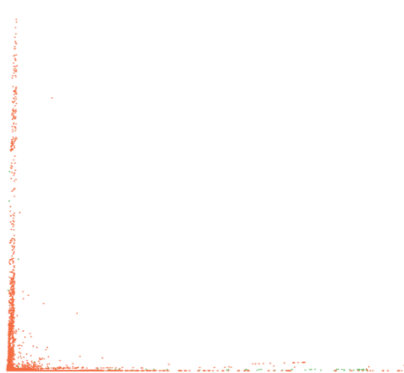


Figure 8: Visualizations of Covertypes and RCV1 datasets using LargeVis, TriMap, and PCA, and visualizations of the Character Font Images dataset using LargeVis, TriMap, and PCA. The values of nearest neighbor accuracy and global score are shown as a tuple (NN, GS) on top of each figure.

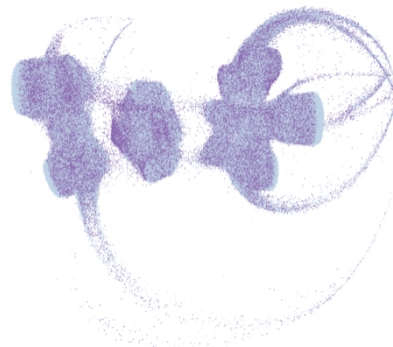
KDDCup99 - TriMap (0.97, 0.00)



KDDCup99 - PCA (0.88, 1.00)



HIGGS - TriMap (0.53, 0.94)



HIGGS - PCA (0.54, 1.00)

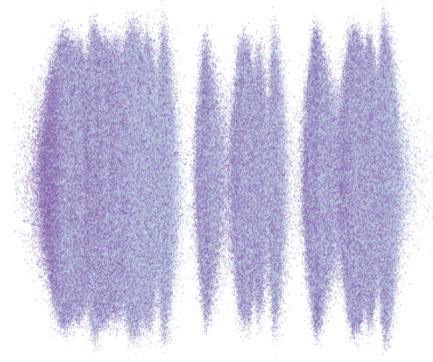


Figure 9: Visualizations of KDDCup99 and HIGGS datasets TriMap and PCA. Each row corresponds to one dataset and each column represents one method. The values of nearest neighbor accuracy and global score are shown as a tuple (NN, GS) on top of each figure. TriMap shows more structure for both datasets than PCA. Note that GS is uninformative for the KDDCup99 dataset.